Supplementary Information for

Vapor–solid–solid growth of single-walled carbon nanotubes

Daniel Hedman

Center for Multidimensional Carbon Materials (CMCM), Institute for Basic Science (IBS),
Ulsan, 44919, Republic of Korea. e-mail: daniel@hedman.science

Here, additional information is presented to support the results in the main text, including the accuracy of $\mathrm{NEP_{ReC}}$, facet-dependent surface energies, size-dependent nanoparticle stability, nanoparticle reconstruction under carbon exposure, nanotube cap nucleation, and chirality-dependent annealing behavior.

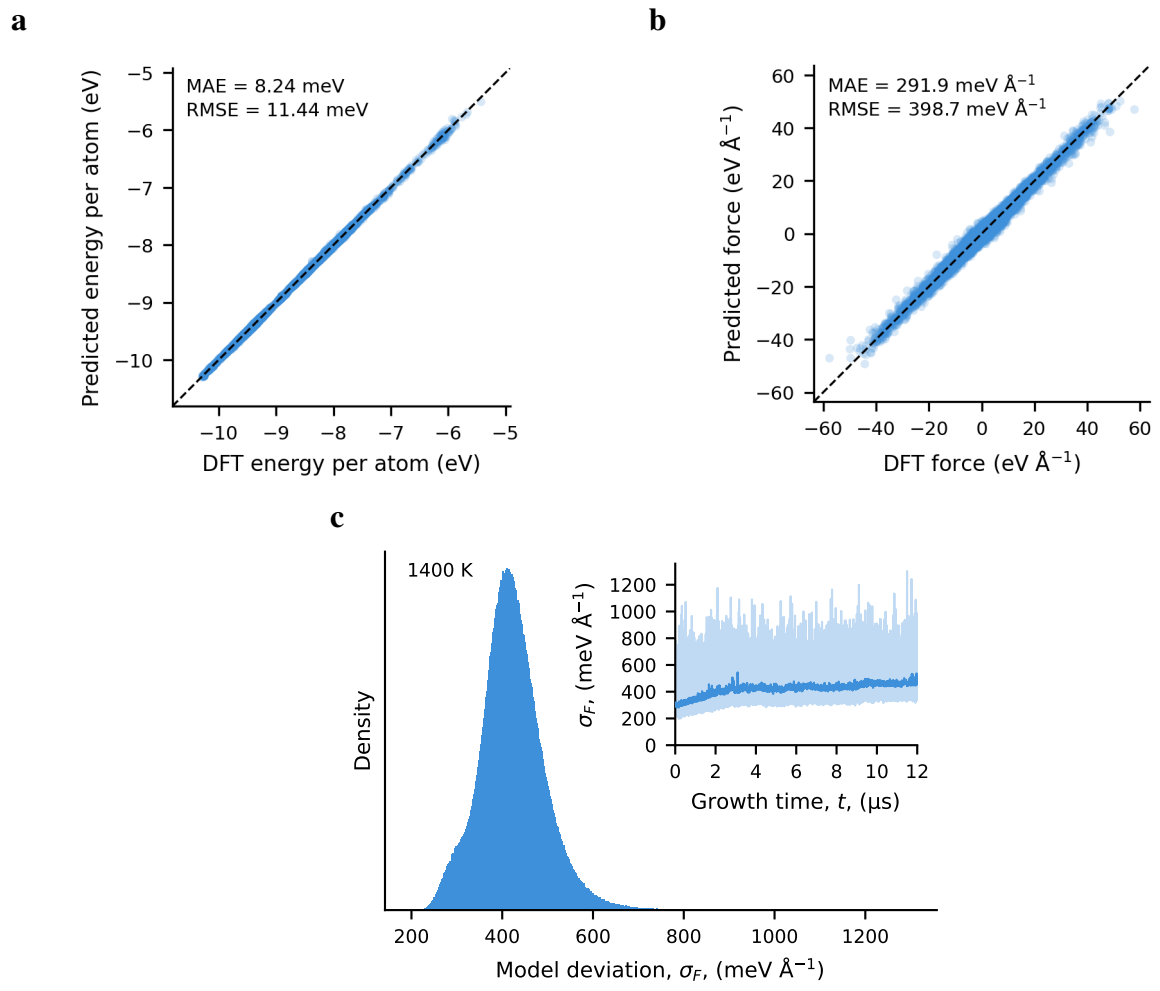

Fig. S1. Accuracy of $\mathrm{NEP_{ReC}}$. **a** comparison of DFT and NEP-predicted energies per atom for the test dataset. **b** comparison of DFT and NEP-predicted atomic forces for the test dataset. **c** maximum force model deviation, σ_F, obtained from the four-member NEP ensemble over the 12 µs growth simulation in Fig. 4. The inset shows the time evolution of σ_F where the transparent lines are raw data and the solid line is averaged over 1 ns blocks. Low model deviation indicates that the simulation remains within the configuration space covered by the actively learned dataset.

Table S1. Surface energies, γ, for rhenium-HCP facets calculated with DFT and NEP_{ReC} for clean surfaces and for surfaces with a carbon coverage of $5.5\,\text{nm}^{-2}$. Relative errors for NEP_{ReC} are given with respect to DFT showing high accuracy. For the Wulff nanoparticles used in this work and the Wulff constructs shown in Figure 2, the DFT-calculated surface energies were used.

	Clean surfaces (no carbon)			Carbon covered surfaces ($5.5\,\text{nm}^{-2}$)		
$(h\,k\,i\,\ell)$	γ_{DFT} (meV Å^{-2})	γ_{NEP} (meV Å^{-2})	Err. (%)	γ_{DFT} (meV Å^{-2})	γ_{NEP} (meV Å^{-2})	Err. (%)
(0001)	188.03	199.53	6.12	214.75	209.05	2.65
$(10\bar{1}0)$	203.07	211.68	4.24	215.95	216.25	0.14
$(11\bar{2}0)$	216.46	233.10	7.69	231.83	238.40	2.83
$(21\bar{3}0)$	219.00	234.98	7.30	228.49	235.28	2.97
$(20\bar{2}1)$	224.67	222.72	0.87	209.43	213.99	2.18
$(22\bar{4}1)$	230.76	239.14	3.63	232.96	241.12	3.50
$(10\bar{1}1)$	230.41	220.14	4.46	187.39	194.86	3.99
$(10\bar{1}2)$	233.14	237.21	1.75	228.70	230.09	0.61
$(21\bar{3}1)$	232.14	236.96	2.08	225.80	233.08	3.22
$(11\bar{2}1)$	236.13	239.78	1.55	240.40	243.15	1.14
$(2\bar{1}\bar{1}2)$	241.57	234.33	3.00	235.54	233.24	0.98
$(21\bar{3}2)$	242.47	239.08	1.40	219.22	225.01	2.64

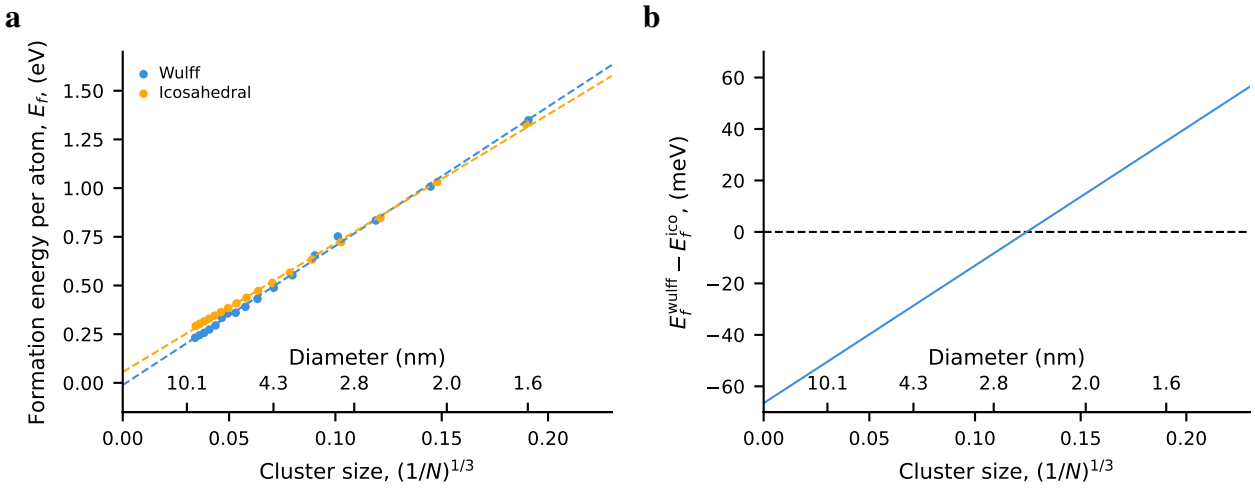

Fig. S2. Size-dependent energetic stability of clean rhenium nanoparticles. **a** formation energy of Wulff and icosahedral Re nanoparticles as a function of particle size. **b** difference in formation energy between the two morphologies, showing the crossover in stability at $\sim 2.4\,\text{nm}$ diameter, above which the Wulff structure is energetically favored. This trend is consistent with the higher melting points of larger Wulff nanoparticles observed in Fig. 2c.

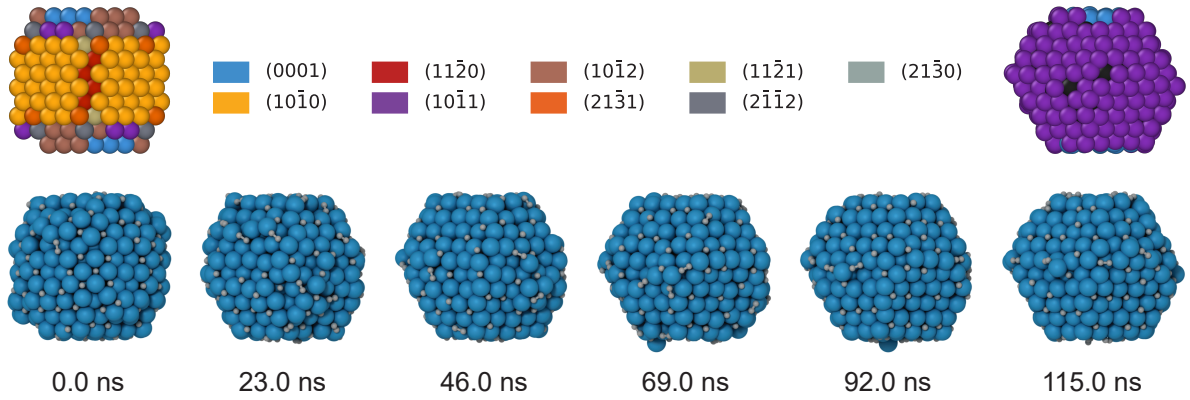

Fig. S3. The reconstruction of the nanoparticle shape due to surface carbon during the first tens of ns of the 12 µs growth simulation in Fig. 4. Here, the colors of the upper left and right nanoparticles indicate which surface each atom is closest to.

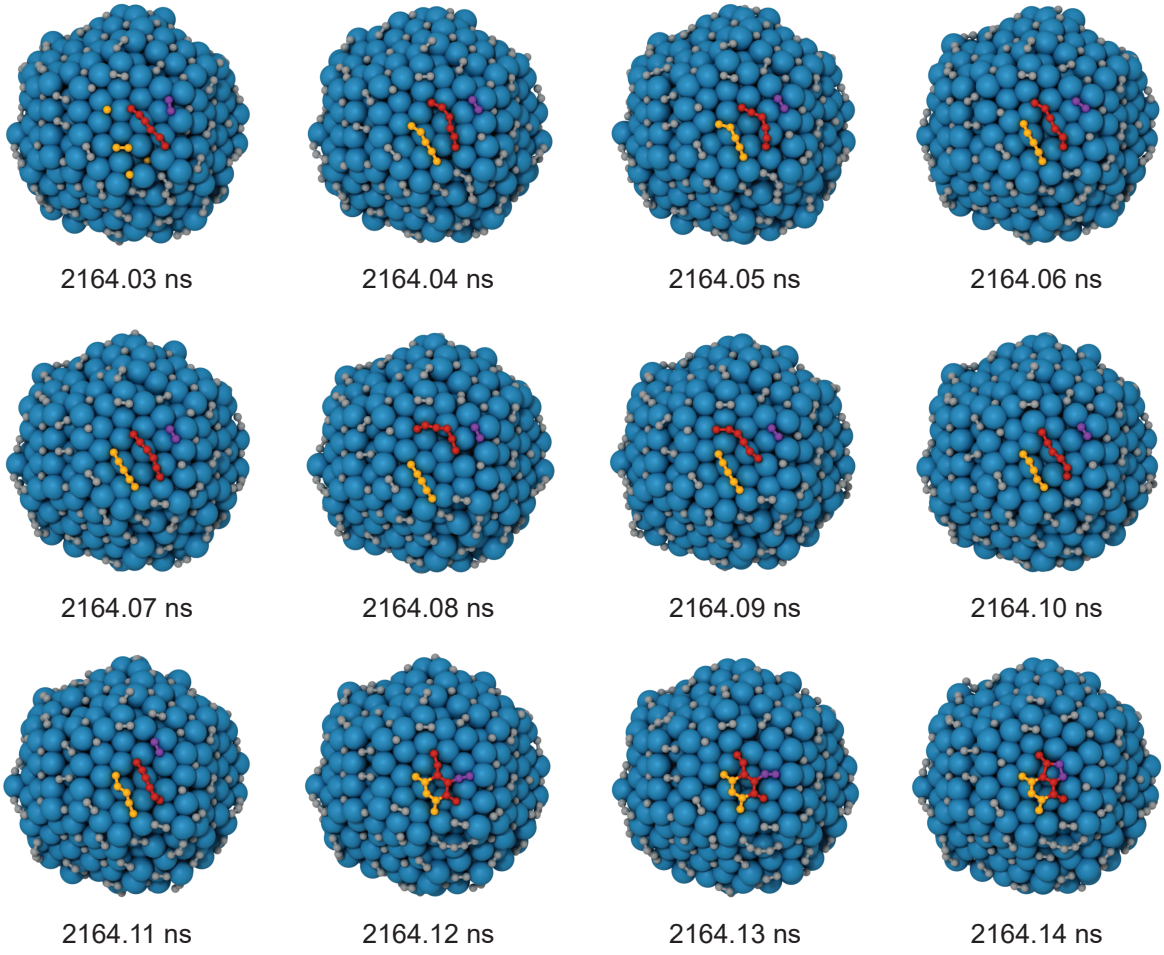

Fig. S4. Snapshots from the 12 µs growth simulation in Fig. 4 showing the nucleation of the first carbon ring that eventually becomes the nanotube cap. Here, the yellow, red, and purple colored atoms represent the carbon atoms that form the nucleus.

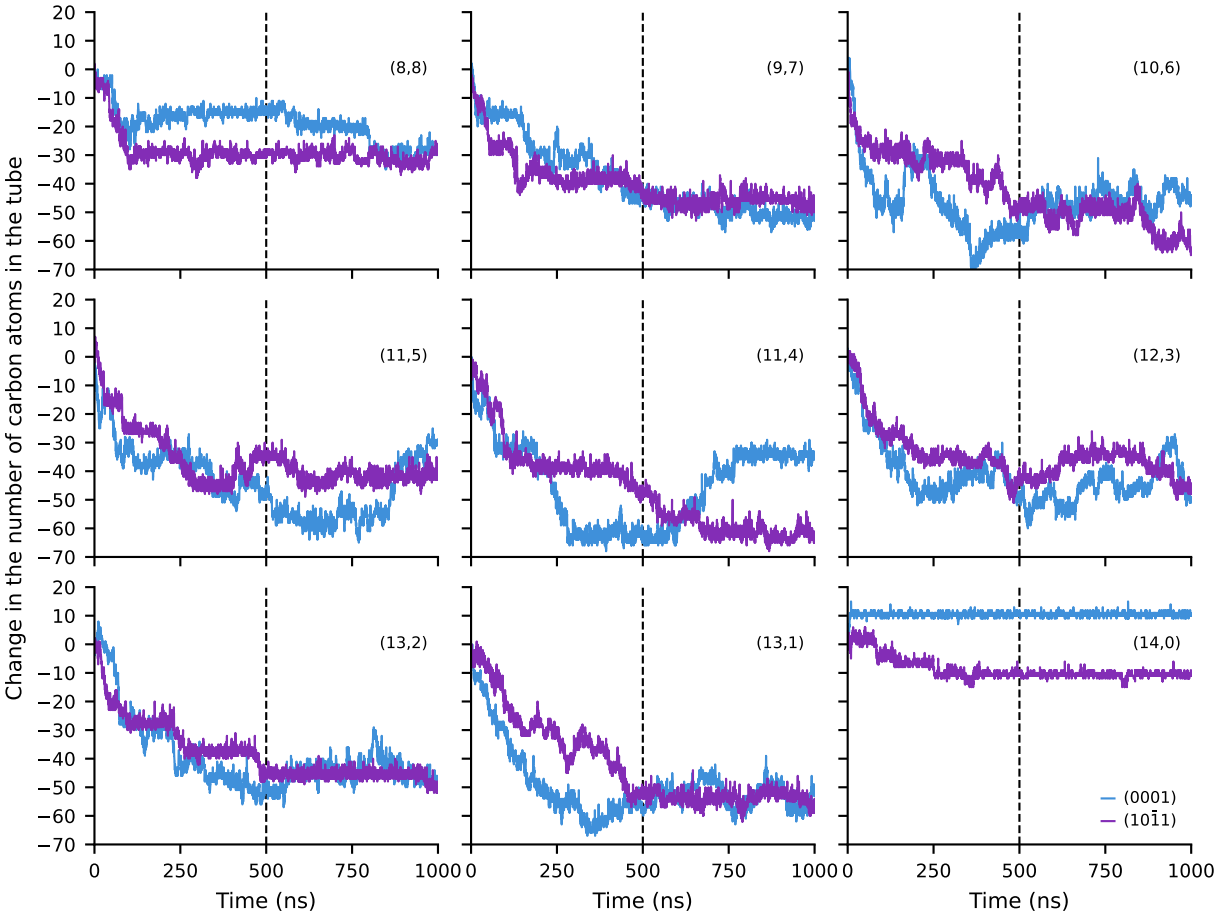

Fig. S5. Change in the number of carbon atoms in the nanotube during 1 µs annealing at 1600 K for SWCNTs attached to Re_{1356} nanoparticles. Results are shown for the chiralities and facet attachments used in Fig. 5b–d. Here, the dashed lines mark where averaging starts, final 500 ns of annealing.